J Mater Sci (2022) 57:589–597

Materials for life science

Gold nanostructures integrated on hollow carbon N-doped nanocapsules as a novel high-performance aptasensing platform for *Helicobacter pylori* detection

Mahmoud Roushani[1,*], Masoumeh Sarabaegi[1], Hadi Hosseini[1], and Fazel Pourahmad[2]

[1] Department of Chemistry, Faculty of Sciences, Ilam University, P. O. Box, 69315-516 Ilam, Iran
[2] Department of Microbiology, Faculty of Veterinary Sciences, Ilam University, P. O. Box 69315-516, Ilam, Iran

Received: 31 July 2021
Accepted: 26 October 2021
Published online: 3 January 2022

ABSTRACT

Nowadays, there is a lot of interest in the design of advanced nanomaterials in the field of electrochemical aptasensors, which can improve analytical performance. In this work, we have established a synthesis of gold nanostructures supported on hollow carbon N-doped nanocapsules (Au@HNC) for the first time. The TEM, Raman, TGA, FE-SEM, XRD, FT-IR, BET, and EDS mapping were used to morphologically study and characterize the as-prepared Au@HNC nanocapsules. The Au@HNC nanocapsules were used for the ultra-sensitive and fast detection of *Helicobacter pylori* taking the virtues of good biocompatibility, high electronic conductivity, and large specific surface area. We designed this platform because one of the most well-known problems in the world is *Helicobacter pylori* infection which causes dangerous stomach diseases. The linearity and detection limit of the Aptamer/Au@HNC aptasensor were found to be 33 CFU mL^{-1} and 10^2 to10^7 CFU mL^{-1} for *Helicobacter pylori*, respectively.

Introduction

Recently, the electrochemical aptasensors have received great attention because of their advantages, including, low cost, simple method, and high sensitivity and selectivity [1–3]. In fact, the function of aptamer is combined with electrochemistry to detect different target molecules. Aptamers, like antibodies, have a strong desire for their targets [4]. Aptamer-based sensors have been greatly applied due to their easy chemical modification, stability, and finesse in the fabrication of nanostructured devices [5]. In recent years, the performance of aptasensors has been enhanced by the incorporation of new nanomaterials [6]. Heretofore, a large number of electrochemical biosensors have been reported using nanomaterials such as quantum dots [7], carbon nanotubes [8] metals [9], metal oxides [10], graphene [11], and their

Handling Editor: Andrea de Camargo.

Address correspondence to E-mail: mahmoudroushani@yahoo.com; m.roushani@ilam.ac.ir

https://doi.org/10.1007/s10853-021-06667-7

derivated nanocomposites [12]. Among the new nanomaterials, carbon nanostructures pave the way for emerging technologies in the field of molecular electronic devices and are widely used in analytical electrochemistry [13, 14]. In addition, the rapid development of nanotechnology has led to the introduction of optimal diagnostic systems through the design of biosensors [15]. In this regard, the intelligent engineering of carbon composite nanostructures—capable of binding specific binders—can increase the practical challenges in aptasensor technology [16]. Among carbon nanostructures, hollow nitrogen-doped carbon nanocapsules derived from the iron oxide pattern can provide an excellent conductive carbon layer for the intelligent engineering of hollow nitrogen-doped carbon (HNC) nanocapsules [17]. The HNC nanocapsules possess useful properties, such as electrical conductivity, large production scale in biosensor development, strong adsorptive ability, low cost, improved electrochemical applications by enabling novel designs in sensing, electronics, and electrocatalysis. The HNC—as compared to graphene and CNTs—has the advantages of high electrical conductivity, small thickness, and large surface area. To improve the function of aptasensors, these HNC nanocapsules can enhance the loading of biomolecules and increase sensitivity. Another factor that can improve the performance of HCN is the integration of HCN with metal nanoparticles, which is usually necessary to enhance the biosensing properties [18]. The metal nanoparticles also increase electrochemical sensitivity. In addition, metal nanomaterials with very special surface are considered as desirable materials, related to the analytical performance of safety sensors [19]. Among all kinds of metal nanoparticles, gold nanoparticles (AuNPs) have been extensively used in fabrication of different kinds of sensors due to their unique structure and fascinating properties, such as high surface-to-volume ratio which facilities binding of biomolecules, as well as direct and strong adsorption ability, good biocompatibility, and conductivity. Impressively, Au, which displays excellent biocompatibility and electrical conductivity, is one of the most broadly adopted nanomaterials [20]. In this sense, it is worth mentioning that the combination of AuNPs with HNC nanocapsules as a new electrode material which can integrate the properties of these materials for electrochemical sensing has not been reported.

Diagnosis of *Helicobacter pylori* (Hp) has become a significant interest due to its ability to cause gastric cancer. Over the past few years, the death rate from gastric cancer has increased dramatically [21]. These spiral-shaped, Gram-negative bacteria are microaerophilic in nature and colonize the inner lining of human stomach [22]. Quantitative standard methods are available for detecting Hp through invasive and noninvasive techniques. But, these methods are time-consuming, costly, labor-intensive, involve time-consuming sample preparation, and lack precision [23]. To overcome these drawbacks, the electrochemical aptasensors have received a lot of attention due to minimal limit of detection, cost-effectiveness, high sensitivity, simple, and fast measurement.

Based on the told preface, herein, we designed a novel necklace-like structure composed of Au@HNC with excellent electron conductivity and a good biocompatibility. The HNC that is derived from the iron oxide pattern can provide an excellent conductive carbon layer for Au attachment. This method is simple and no toxic organic solvent and special apparatus is involved. Moreover, L-ascorbic acid which is an important biomolecule can be employed as an eco-friendly reducing agent. The Au@HNC nanocapsule acts as an excellent substrate with high surface for binding aptamer to the surface of a gold electrode to detect Hp. This is the first report on the rational design of hollow carbonaceous materials hybridized AuNPs for the electrochemical application.

Materials and methods

In this study, the Hp aptamer sequence (5′-AGTGT GCTCTTCTCAGGTCTCGGCGCGGTTGTGGGTAC CTAGGGTTGTTGTTGCTTCTCAGCAGTGTCTCAG CATACGCA-3′) [24] was obtained from the Bioneer Company (South Korea, http://www.bioneer.com). The Hp and all other bacteria used in this study, including *Campylobacter jejuni*, *Campylobacter fetus*, *Vibrio cholerae*, and *Staphylococcus aureus*, were obtained by the Department of Microbiology (Ilam University, Iran). Dopamine, ascorbic acid, $FeCl_3$-$6H_2O$, and NaOH were obtained from Merck or Fluka. The phosphate buffer solution (PBS) and $HAucl_4.\times H_2O$ were bought from Sigma-Aldrich. The electrochemical impedance spectroscopy (EIS) and cyclic voltammetry (CV) were achieved using

μ-AUTOLAB type III computer controlled Potentiostat/Galvanostat (ECO-Chemie, Switzerland). The morphological and composition analysis of the Au@HNC nanocapsules was carried out using *transmission electron microscopy* (TEM: PHILIPS CM300), Brunauer–Emmett–Teller (BET; Bruker; Model—Belsorp miniII), Fourier transform infrared spectroscopy (FTIR; Bruker; Model-VERTEX 70), field emission scanning electron microscopy (FE-SEM; TSCAN, Czechia), and X-ray diffraction measurements (XRD; PHILIPS, λ = 1.54 Å).

The preparation of synthesized hollow carbon N-doped nanocapsules

To prepare the Fe_2O_3 nanocapsules, the hydrothermal method was used. In this sense, we first stirred 100 mL solutions of 2.0 M iron (III) chloride in an oil bath at 75 °C for 5 min and, then, slowly added 100 mL of 5.4 M sodium hydroxide solution. In addition, it remained at the same temperature for 75 min, which was obtained as a result of Fe $(OH)_3$ gel, placed in autoclave at 100 °C for 4 days. The product was then centrifuged and dried in a 60 °C oven, to be used in later steps. Afterward, 320 mg of the Fe_2O_3 nanocapsules template was dissolved in Tris-buffer solution. Subsequently, 160 mg of dopamine was added and, then, it was stirred for 3 h. The Fe_2O_3@PDA product was separated from the solvent by centrifugation and, then, dried in an oven at 60 °C to be used in the next step. Afterward, 160 mg of the Fe_2O_3@PDA product was annealed at 500 °C for 3 h in N_2. The product was then used in 4 M hydrochloric acid to remove the template. The hollow carbon N-doped (CN) nanocapsules product was separated from the solvent by centrifugation and, then, dried in a 60 °C oven for later steps.

Preparation of Au@HNC nanocapsule

To prepare the Au@HNC nanocapsule, 43.06 mg of CN nanocapsules was first dissolved in 20 mL of water under intense steering and, then, 50 mmol L^{-1} (0.8 mL) of $HAuCl_4.XH_2O$ was added. In the next step, 1.00 mL of L-ascorbic acid was slowly added dropwise to the mentioned solution, which was placed at 70 °C for 2 h. After cooling to ambient temperature, the precipitate was separated from the solvent by centrifugation at 12000 rpm and, then, placed in an oven to dry at 60 °C.

Preparation of the Bacteria

All bacteria were cultured in LB broth and, then, incubated for 18 h at 37 °C. Bacteria used in this article include *Campylobacter jejuni*, *Campylobacter fetus*, *Vibrio cholerae*, *Staphylococcus aureus*, and Hp. All bacterial dilutions were performed at PBS (pH 7.4).

Preparation of the biosensor

The gold electrode was first polished on 0.05 μm alumina slurry and, then, cleaned by CV 10 cycles, between − 0.4 and − 1.6 V, and 0.05 V s^{-1} in 0.5 M NaOH. It was then polished again with alumina and thoroughly washed ultrasonically in ultrapure water and ethanol. In the final step of cleaning the electrode, it was electrochemically polished 10 cycles from − 0.3 to 1.7 V, 0.3 V s^{-1} in 1 M H_2SO_4.

In order to prepare the biosensor; first, 10 μL of Au@HNC nanocapsule ink was injected on the surface of the gold electrode. Subsequently, the Au@HNC/Au was dried in the room temperature. In the final step of biosensor preparation, 10 μL of aptamer (2 μM) was injected on the surface of the Au@HNC/Au for 24 h at 4 °C through stabilizing the aptamer NH_2 group to the Au in the nanocomposite. The Aptamer/Au@HNC/Au was estimated with different concentrations of Hp. The preparation of the biosensor is shown in Fig. 1B.

Results and discussion

Surface characterization

The preparation method of Au@HNC nanocapsules is schematically shown in Fig. 1A. The uniform Fe_2O_3 nanocapsules are easily prepared by a simple hydrothermal method (Fig. 1A(a)). Afterward, the collected Fe_2O_3 nanocapsules were uniformly coated with the poly dopamine layer and, then, carbonized under N_2 atmosphere at 500° C to convert the poly dopamine layer to the carbon N-doped layer (Fig. 1A(b)). In the next step (Fig. 1A(c)), the Fe-oxide core was completely and selectively removed by etching in HCl acid. Consequently, HNC nanocapsules were obtained. In the final step, the Au nanoparticles were formed on HNC nanocapsule to obtain Au@HNC nanocapsule. The as-prepared

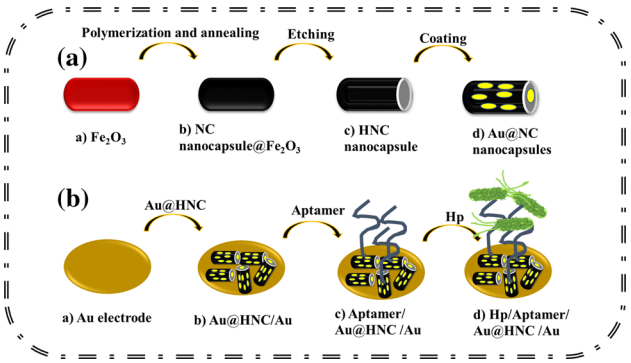

Figure 1 Schematic representation of the preparation of **a** Au@HNC nanocapsule and **b** the proposed Hp aptasensor.

materials at different stages are rigorously characterized and analyzed using TEM, FESEM, EDX, MAP, XRD, TGA, BET, FTIR, and Raman spectroscopy.

The FESEM was used in the preparation of Au@HNC nanocapsule for the structural and morphological studies. Highly uniform Fe_2O_3 nanocapsules are formed as the template through a simple hydrothermal method Fig. 2a, b. As you can see in Fig. 2c, d, the structure is preserved after the removal of iron oxide and the average size of HNC nanocapsules (about 650 nm) corresponds to the size of Fe_2O_3 nanocapsule. The FESEM images of Au@HNC nanocapsule (Fig. 2e, f) showed that the structure of HNC nanocapsules has been maintained. Moreover, the EDX elemental mapping images and EDX spectra of the Au@HNC nanocapsule show the presence and uniform distribution of the Au, N, and C in Au@HNC nanocapsule (Fig. 3).

To better confirm the formation of AuNPs on HNCs HNC nanocapsule, the TEM technique was applied. As shown in Fig. 4a, the TEM image of HNC nanocapsule clearly shows the hollow structure. The TEM images of Au@HNC nanocapsule, which illustrate the presence of some black dots with an average size of about 37 nm on the HNC nanocapsule, can be related to the formation of AuNPs confirming the synthesis of AuNPs on HNC nanocapsule Fig. 4b–d.

The XRD analysis was implemented to identify the crystal structures of the Au@HNC nanocapsule. The diffraction peaks of the Fe_2O_3 nanocapsules template can be excellently matched to the rhombohedral Fe_2O_3 (JCPDS 00-013-0534) with cell parameters of a = 5.0310 Å, b = 5.0310 Å, and c = 13.7370 Å, confirming the successful preparation of Fe_2O_3 nanocapsules with high pure crystalline nature Fig. 5 a. The three diffraction peaks at 2θ values of 39.16°, 44.69°, and 65.76° (Fig. 5b) are assigned to the (111), (200), and (220) planes of pure Au (JCPDS 00-001-1172), further proving the efficient formation of the Au@HNC nanocapsule [25].

In addition, the pore size and surface area of the Au@HNC nanocapsule were evaluated using the pore size distribution diagram and N_2 adsorption and desorption isotherm (Fig. 1S). Besides, the BET surface area is 64.46 $m^2\ g^{-1}$ for the Au@HNC nanocapsule, which is a high surface area for Au-based carbon nanomaterials. A typical type IV plot was observed for the Au@HNC nanocapsule, which indicates the existence of mesopores in the Au@HNC nanocapsule (Fig. 1S). Furthermore, the Au@HNC nanocapsule pore size distribution confirms a pores majority between 1 to 3 nm (Fig. 1S inset).

The Raman technique was used to further identify the structures. Figure 6A.a shows the Raman spectra

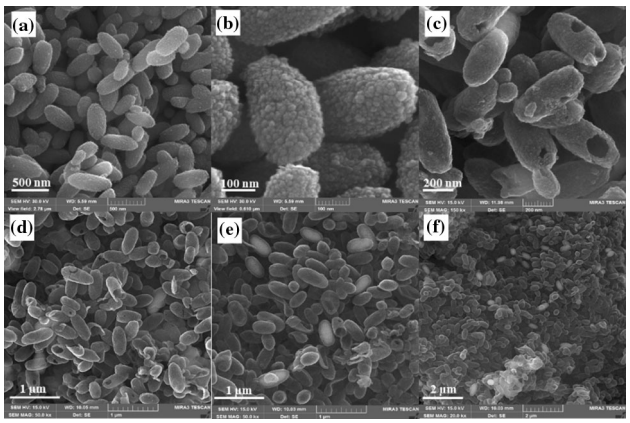

Figure 2 The FESEM images of **a**, **b** Fe_2O_3 nanocapsule, **c**, **d** N–C nanocapsule and **e**, **f** Au@HNC nanocapsule.

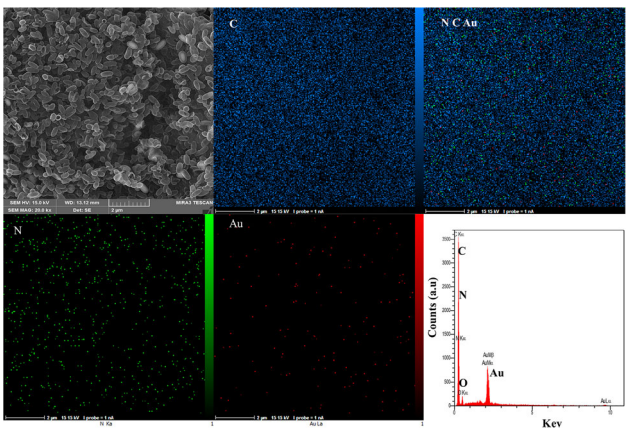

Figure 3 EDS spectrum and EDS map of element distribution in the Au@HNC nanocapsule.

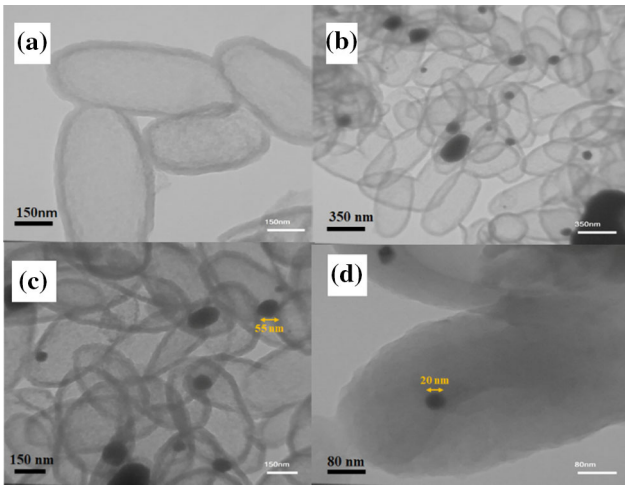

Figure 4 The TEM images of **a** HNC nanocapsule and **b–d** Au@HNC nanocapsule.

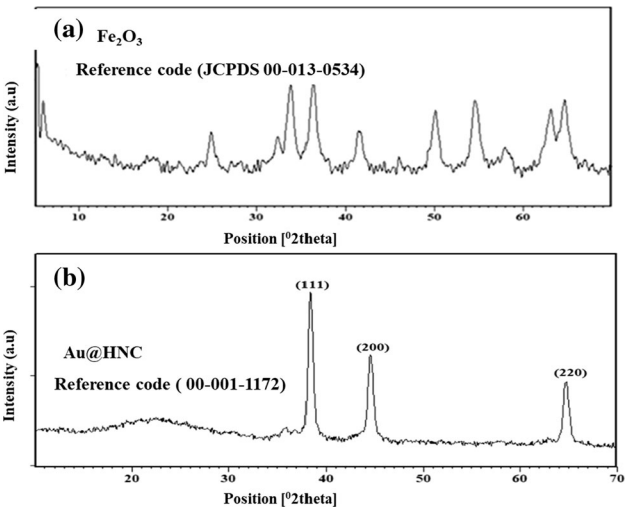

Figure 5 The XRD patterns of the synthesized **a** Fe_2O_3 nanocapsule, **b** Au@HNC nanocapsule.

of HNC (black curve) and Au@HNC nanocapsule (red curve). The Raman pattern of HNC which is matched with the Raman spectra of carbon-based compounds shows the D band (~ 1360 cm^{-1}) and G band (~ 1570 cm^{-1}) [26]. After the formation of Au nanoparticles on HNC nanocapsule, an increase in the ratios of I_D/I_G peak intensity of Au@HNC nanocapsule (0.8) was observed compared with bare HNC (0.75), illustrating an increase in the edge defects due to the formation of Au nanoparticles.

Figure 2S. (A) indicates the TGA curves of (a) HNC nanocapsule and (b) Au@HNC nanocapsule. The TGA of Au@HNC nanocapsule was compared to HNC. The HNC begins to decompose at about 380° C

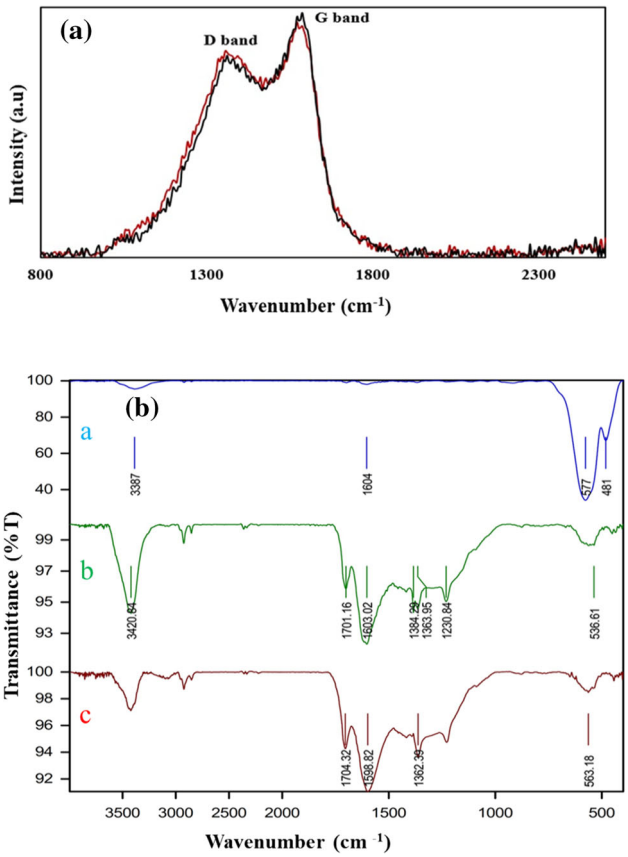

Figure 6 **A** The FTIR spectra of **a** Fe_2O_3 nanocapsule, **b** HNC nanocapsule, and **c** Au@HNC nanocapsule. **B** The Raman spectra of HNC (black curve) and Au@HNC nanocapsule (red curve).

and burned completely above 580 °C and the remaining weight is almost zero percent. For the Au@HNC nanocapsule, it was revealed that the remaining twenty percent can be related to the loading of Au NPs in the HNC structure.

The FTIR spectra of (a) Fe_2O_3 nanocapsule, (b) HNC nanocapsule, and (c) Au@HNC nanocapsule were studied. As shown in Fig. 6B (curve a), the region between 450 and 600 cm^{-1} illustrated the Fe–O stretching. After removing the Fe–O core and carbonization, the region between 450 and 600 cm^{-1} seems to have been disappeared and, instead, new vibration peaks are appeared which can be regarded as the characteristic of HNC nanocapsule Fig. 6B(b) [27]. After the formation of Au nanoparticles in the HNC nanocapsule, the peaks of Au@HNC nanocapsule are shifted, as compared to the peaks of HNC nanocapsule (Fig. 6B(c)) [28].

The cyclic voltammetry (CV) is one of the most significant ways to find out if gold nanoparticles are on the electrode surface, using an Ag/AgCl/sat., KCl

as reference electrode, platinum as counter electrode, and glassy carbon modified with (a) HNC nanocapsule and (b) Au@HNC nanocapsule as working electrode in sulfuric acid solution, and in the potential range between − 0.2 and 1.2 V. As can be seen in Fig. 3S. CV of (b) Au@HNC nanocapsule as compared to (a) HNC nanocapsule, the redox peak confirms that there is a gold nanoparticle on the electrode surface [29].

Characterization and the electrochemical behavior of the aptasensing of Hp

The unparalleled appealing of hollow and mesoporous structure with superior composition can offer the Au@HNC nanocapsule as a high-performance electrode material for biosensing application. In this sense, the performance of Hp /Aptamer/Au@HNC/Au was evaluated by CV and EIS. The CV obtained from different steps of electrode surface modification in $Fe(CN)_6]^{3-}$ /$[Fe(CN)_6]^{4-}$ solution is shown in Fig. 7A. According to this Fig. 7A (curve a), the unmodified Au electrode shows the highest peak current. In this regard after modifying the surface of the electrode with Au@HNC nanocapsule, the peak currents of the probe increased on the surface of Au@HNC nanocapsule Fig. 7A (curve b). This might be due to the fact that CN ligand in Fe $(CN)_6]^{3-}$/[Fe $(CN)_6]^{4-}$ can also coordinate with AuNPs, which might reduce the electron-tunneling distance for Fe $(CN)_6]^{3-}$/[Fe $(CN)_6]^{4-}$. Thus, the modification of the Au electrode by Au@HNC actually improved the electron transfer properties of the modified electrode and, accordingly, the peak currents for Au electrode modified Au@HNC electrode increased.

Subsequently, in the next step, after modifying the surface of the electrode (Au@HNC/Au) immobilized with aptamer on its surface, the oxidation and reduction peak current became less than that of the Au@HNC nanocapsule (curve c). This is due to the fact that it was difficult to exchange electrons between the $Fe(CN)_6]^{3-}$/$[Fe(CN)_6]^{4-}$ and the modified electrode.

In the final step, by incubating the Hp, the peak current decreased again (curve d). This phenomenon is due to the analyte connection to the aptamer, by which a barrier is created as a complex between the Hp and the aptamer. Moreover, further blockage of the surface and inhibition of electron transfer, by the

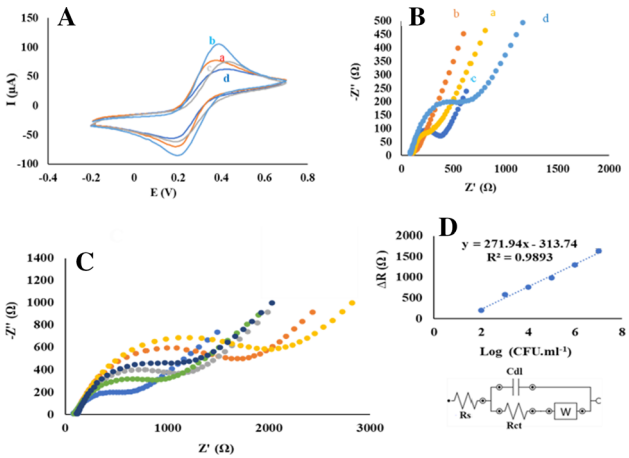

Figure 7 **A** Recorded CVs of the modified electrode after each immobilization **a** Au electrode, **b** Au@HNC/Au, **c** Aptamer/Au@HNC/Au, and **d** Hp/Aptamer/Au@HNC/Au. **B** Nyquist curves for the different steps of the modified electrode: **a**–**d** are the same as (**A**). **C**The inset is the equivalent circuit and EIS response of electrochemical aptasensor and calibration curve with increasing Hp concentration is at 10^2, 10^3, 10^4, 10^5, 10^6, and 10^7 CFU mL^{-1} of the impedance aptasensor for detecting Hp. All of them were recorded in a solution containing 5 mM $Fe(CN)_6^{3-/4-}$ and 0.1 M KCl.

probe species and the electrode surface, are witnessed.

The EIS was also applied to different steps of electrode surface modification in $Fe(CN)_6]^{3-}$/$[Fe(CN)_6]^{4-}$ solution, as shown in (Fig. 7B). According to Fig. 7B (curve b), it can be seen that the Rct curve (b) corresponds to the decreased substrate Au@HNC nanocapsule as compared to the value of the Rct curve (a) of the bare Au electrode, indicating that Au@HNC nanocapsule covers the surface of the electrode.

As shown in Fig. 7B, the Rct (curve c) for Aptamer/Au@HNC/Au increased as compared to the Au@HNC nanocapsule/Au (curve b). This is due to the stabilization of the aptamer on the substrate through the binding of the aptamer NH_2 group to the nanocomposite. By attaching the aptamer to the substrate, more space is created and electron transfer between the electrode surface and the probe species is reduced. The Rct (curve d), which is related to the incubation of the Hp (10^2 CFU mL^{-1}), is associated with an increase in Rct as compared to the previous curves, indicating the successful adsorption of the Hp on the aptamer. As a result, according to Fig. 7, the

Table 1 Detection of Hp in blood serum samples ($n = 3$)

Sample	Added value (CFU mL^{-1})	Detected (CFU mL^{-1})	Recovery (%)	RSD (%)
1	10^3	$1.120 \times 10^3(\pm 0.06)$	112.00	3.90
2	10^5	$0.994 \times 10^5(\pm 0.03)$	99.40	2.80
3	10^7	$0.998 \times 10^7(\pm 0.02)$	99.80	2.30

CV and EIS confirm the correctness of the electrode surface correction process.

Investigation of the Analytical application of the Hp aptasensor

The relationship between Hp concentration and electrochemical signals was studied to confirm the analytical efficiency of the Aptamer/Au@HNC/Au in the detection of Hp. In this study, the EIS technique was used, where Rct is the electron transfer resistance, Zw is the Warburg impedance, Rs is the soluble resistance, and Cdl is the dual-layer capacitance (inner Fig. 7C).

To investigate the best time required for the interaction of Hp and aptamer as the bioreceptor, the time was incubated with 10^6 CFU mL^{-1} Hp at different times of 5, 10, 20, 30 min. According to the results in Fig. 4S, no significant increase in aptasensor response was observed after 20 min; therefore, an incubation time of 20 min was selected. Afterward, different concentrations of Hp were incubated on surface of the Aptamer/Au@HNC/Au for 20 min (10^2, 10^3, 10^4, 10^5, 10^6, and 10^7 CFU mL^{-1}). According to Fig. 7C, while increasing the concentration of Hp, the Rct also increased. As shown in Fig. 7C, the aptasensor shows a linear range with the Hp concentration: the equation is as follows, $y = 271.94 \times - 313.74$ ($R^2 = 0.9899$) and the LOD is 33 CFU mL^{-1}. These results are due to the large area created by the hollow nanocapsule structures and the presence of a gold layer for effective binding of the NH_2 aptamer group and also stabilization of the aptamer to the surface that confirms the performance of our proposed aptasensor.

The selectivity and reproducibility

To evaluate the aptasensor selectivity, the EIS was studied in the presence of *Campylobacter jejuni*, *Campylobacter fetus*, *Vibrio cholerae*, *Staphylococcus aureus, and Hp* (Fig. 5S). As shown in the Figure, the aptasensor is more selective to Hp than other bacteria. In addition, to measure the reproducibility of the aptasensor, Apt/Au@HNC /Au with a concentration of 10^6 CFU mL^{-1} Hp in the same conditions was studied by EIS method (Fig. 6S). The RSD for the obtained values was calculated to be 2.28%, which confirms the accuracy and repeatability of the aptasensor.

Application of the aptasensor for Hp detection in serum samples

The aptasensor evaluation for Hp detection in serum samples was investigated by standard addition methods. In this sense, 0.5 mL of serum sample was added to 1.5 mL of water and three different concentrations of Hp (10^3 CFU mL^{-1}, 10^5 CFU mL^{-1}, and 10^7 CFU mL^{-1}) were added to the diluted serum sample. Moreover, the EIS technique was used. As can be seen in the table, the results of this experiment are given Table 1.

Conclusion

In this work, a novel aptasensor substrate based on gold nanostructures supported on hollow carbon N-doped nanocapsules (Au@HNC) was fabricated for the first time (Au@HNC). Herein, according to the results, without using special apparatus and toxic organic solvent, a novel method was employed as an eco-friendly reducing agent. The aptasensor for Hp was efficiently produced by Au@HNC nanocapsule for their excellent characteristics such as large specific surface area, excellent biocompatibility, suitable substrate for aptamer fixation, abundant catalytic active sites, and high selectivity and sensitivity for the Hp target. Therefore, for the first time, this research demonstrates the fabrication and use of hollow gold nanofibers/carbon nanostructures for the field of biosensor and also introduces the fabrication and use of gold nanostructures supported on hollow carbon N-doped nanocapsules (Au@HNC) for biosensing field.

Supplementary Information: The online version contains supplementary material available at https://doi.org/10.1007/s10853-021-06667-7.

References

[1] Wang L, Peng X, Fu H, Huang Li Y, Liu Z (2020) Recent advances in the development of electrochemical aptasensors for detection of heavy metals in food. Biosens Bioelectron147:111777

[2] Li Y, Wang X, Gao L, Hu P, Jiang L, Ren T, Fu R, Yang D, Jiang X (2018) Aptamer-conjugated gold nanostars for targeted cancer photothermal therapy. J Mater Sci 53:14148–14148. https://doi.org/10.1007/s10853-018-2668-7

[3] Yao Y, Wang GX, Shi XJ, Li JS, Yang FZ, Cheng ST, Zhang H, Dong HW, Guo YM, Sun X, Wu YX (2020) Ultrasensitive aptamer-based biosensor for acetamiprid using tetrahedral DNA nanostructures. J Mater Sci 55:15975–15987. https://doi.org/10.1007/s10853-020-05132-1

[4] Negahdary M (2020) Electrochemical aptasensors based on the gold nanostructures. Talanta 216:120999

[5] Kudłak B, Wieczerzak M (2020) Aptamer based tools for environmental and therapeutic monitoring: a review of developments, applications, future perspectives. Crit Rev Env Sci Tech 50:816–867

[6] Antunes D, Jorge NA, Caffarena ER, Passetti F (2018) Using RNA sequence and structure for the prediction of riboswitch aptamer: a comprehensive review of available software and tools. Front Genet 8:231

[7] Zhao J, Chen G, Zhu L, Li G (2011) Graphene quantum dots-based platform for the fabrication of electrochemical biosensors. Electrochem commun 13:131–133

[8] Gupta S, Murthy CN, RatnaPrabha C (2018) Recent advances in carbon nanotube based electrochemical biosensors. Int J Biol Macromol 108:687–703

[9] Wang Y, Huang K, Wu X (2017) Mesoporous materials-based electrochemical biosensors from enzymatic to nonenzymatic. Biosens Bioelectron 97:305–316

[10] Shetti NP, Bukkitgar SD, Reddy KR, Reddy CV, Aminabhavi TM (2019) Nanostructured titanium oxide hybrids-based electrochemial biosensors for healthcare applications. Colloids Surf B 178:385–394

[11] Fang Y, Wang E (2013) Electrochemical biosensors on platforms of graphene. Chem Commun 49:9526–9539

[12] Wang L, Zhang Q, Chen S, Xu F, Chen S, Jia J, Tan H, Hou H, Song Y (2014) Electrochemical sensing and biosensing platform based on biomass-derived macroporous carbon materials. Anal Chem 86(3):1414–1421

[13] Cao M-S, Wang X-X, Zhang M, Shu J-C, Cao W-Q, Yang H-J, Fang X-Y, Yuan J (2020) Electromagnetic response and energy conversion for functions and devices in low-dimensional materials. Adv Mater 32(10):1907156

[14] Cao M-S, Wang X-X, Zhang M, Shu J-C, Cao W-Q, Yang H-J, Fang X-Y, Yuan J (2019) Electromagnetic, response and energy conversion for functions and devices in low-dimensional materials. Adv Funct Mater 29(25):1807398

[15] Maehashi K, Matsumoto K (2009) Label-free electrical detection using carbon nanotube-based, biosensors. Sensors 9:5368–5378

[16] Sarabaegi M, Roushani M, Hosseini H (2021) Hollow carbon nanocapsules-based nitrogen-doped carbon nanofibers with rosary-like structure as a high surface substrate for impedimetric detection of Pseudomonas aeruginosa. Talanta 223:121700

[17] Hosseini H, Roushani M (2020) Rational design of hollow core-double shells hybrid nanoboxes and nanopipes composed of hierarchical Cu-Ni-Co selenides anchored on nitrogen-doped carbon skeletons as efficient and stable bifunctional electrocatalysts for overall water splitting. Chem Eng J 402:126174

[18] Cen S, Feng Y, Zhu J, Wang X, Wang A, Luo X, Feng J (2021) Eco-friendly one-pot aqueous synthesis of ultra-thin AuPdCu alloyed nanowire-like networks for highly sensitive immunoassay of creatine kinase-MB. Sens Actuators B Chem 333:129573

[19] Rawal R, Chawla S, Dahiya T, Pundir C (2011) Development of an amperometric sulfite biosensor based on a gold nanoparticles/chitosan/multiwalled carbon nanotubes/polyaniline-modified gold electrode. Anal Bioanal Chem 401:2599–2608

[20] Rezaei B, Boroujeni M, Ensafi A (2014) Caffeine electrochemical sensor using imprinted film as recognition element based on polypyrrole, sol-gel, and gold nanoparticles hybrid nanocomposite modified pencil graphite electrode. Biosens Bioelectron 60:77–83

[21] Chauhan N, Gupta S, Avasthi D, Adelung R, Mishra Y, Jain U (2018) Zinc oxide tetrapods based biohybrid interface for voltammetric sensing of Helicobacter pylori. ACS Appl Mater Interf 36:30631–30639

[22] Liu Z, Su X (2017) A novel fluorescent DNA sensor for ultrasensitive detection of Helicobacter pylori. Biosens Bioelectron 87:66–72

[23] Guptaa S, Tiwarib A, Jaina U, Chauhan N (2019) Synergistic effect of 2D material coated Pt nanoparticles with PEDOT polymer on electrode surface interface for a sensitive label free Helicobacter pylori CagA(Ag-Ab) immunosensing. Mater Sci Eng C 103:109733

[24] Gu L, Ren W, Ma X, Qin M, Lyu M, Wang S (2019) Recognition of *Helicobacter pylori* by protein-targeting aptamers. Helicobacter 24:12577

[25] Wang QL, Fang R, He LL, Feng JJ, Yuan JH, Wang AJ (2016) Bimetallic PdAu alloyed nanowires: Rapid synthesis via oriented attachment growth and their high electrocatalytic activity for methanol oxidation reaction. J Alloys Compd 684(25):379–388

[26] Roushani M, Hosseini H, Hajinia Z, Rahmati Z, (2021) Rationally designed of hollow nitrogen doped carbon nanotubes double shelled with hierarchical nickel hydroxide nanosheet as a high performance surface substrate for cortisol aptasensing. Electrochim Acta 388:138608

[27] Roushani M, Sarabaegi M, Hosseini H (2021) Flexible NiP_2@hollow N-doped nanocapsules/carbon nanofiber as a freestanding electrode for glucose sensing. Compos Commun 25:100686

[28] Badia A, Cuccia L, Demers L, Morin F, Lennox RB (1997) Structure and dynamics in alkanethiolate monolayers self-assembled on gold nanoparticles: A DSC, FT-IR, and deuterium NMR study. J Am Chem Soc 119:2682–2692

[29] Xu X, Makaraviciute A, Pettersson J, Zhang SL , Nyholm L, Zhang Z (2019) Revisiting the factors influencing gold electrodes prepared using cyclic voltammetry 283:146–153